Applied Catalysis A: General 467 (2013) 552–558

Contents lists available at ScienceDirect

Applied Catalysis A: General

journal homepage: www.elsevier.com/locate/apcata

Influence of the operating conditions and kinetic analysis of the selective hydrogenation of oleic acid on Ru–Sn–B/Al_2O_3 catalysts

María A. Sánchez [a], Yannick Pouilloux [b], Vanina A. Mazzieri [a], Carlos L. Pieck [a,*]

[a] Instituto de Investigaciones en Catálisis y Petroquímica (INCAPE) (FIQ-UNL, CONICET), Santiago del Estero 2654, S3000AOJ Santa Fe, Argentina
[b] Institut de Chimie des Milieux et Matériaux de Poitiers (IC2MP), UMR 6503, CNRS – Université de Poitiers, 4 rue Michel Brunet, 860022 Poitiers Cedex, France

ARTICLE INFO

Article history:
Received 8 May 2013
Received in revised form 2 August 2013
Accepted 9 August 2013
Available online xxx

Keywords:
Ru–Sn–B/Al_2O_3
Selective hydrogenation
Oleic acid
Oleyl alcohol

ABSTRACT

The influence of the operating conditions on the selectivity and activity of Ru–Sn–B/Al_2O_3 catalysts for the hydrogenation of oleic acid to oleyl alcohol was studied. It was found that the Ru–Sn–B/Al_2O_3 catalyst is selective to oleyl alcohol while Ru or Ru–B/Al_2O_3 catalysts are not selective to produce oleyl alcohol. The electronic and catalytic properties of Ru are modified by the strong interaction between Sn and B. The incorporation of Sn leads to catalysts capable of producing oleyl alcohol.

The experiments of oleic acid hydrogenation showed that an increase in reaction temperature leads to an increase in activity while the selectivity to oleyl alcohol goes through a maximum. This is because the reactions of hydrogenation of C=C double bond have lower activation energies than hydrogenolytic reactions. The increase in operating pressure has a positive effect on conversion and a more important effect on selectivity. A very simple first order kinetic model is proposed and reasonably represents the results obtained. This model can be useful to compare catalyst performance more rationally.

1. Introduction

The industrial importance of fatty alcohols is due to the large number of reactions in which the hydroxyl group can participate. They are used in cosmetic emulsions (creams, lotions, etc.) to provide consistency; they are also used in industrial emulsions as solubilizers or co-surfactants. The polar nature of these molecules allows alcohols to be used as lubricants in polymer processing or as feedstock for waxes and creams in technical applications (ester waxes). Another industrial area in which the derivatives from fatty alcohols are used is in fragrances and flavors.

The hydrogenation of fatty acid methyl esters for the production of long chain fatty alcohols is a well-known process technology, which has remained largely unchanged over the past decades [1]. The processes for hydrogenating unsaturated fatty alcohols are currently performed at 250–280 °C and 200–250 atm. The commercial catalysts include ZnO, Al_2O_3, Cr_2O_3, Fe_2O_3, and possibly other promoters [2–9]. Some patents have presented new catalysts for selective hydrogenation but they have not been commercially implemented [10–15]. The use of esters presents certain problems because additional steps of esterification and separation must be used. However, methyl esters are currently produced in large quantities for biofuels using methanol as raw material. For this reason, it has been proposed to obtain fatty alcohols from fatty acid hydrogenation.

The transformation of oleic acid to oleyl alcohol is a problem of carbonyl group hydrogenation in the presence of the C=C double bond. The selective catalytic hydrogenation of the carbonyl group in the vicinity of the C=C double bond (conjugated or isolated) is usually conducted by Group VIII metals (Pt, Rh, Ru, etc.). The performance of these catalysts can be improved through the use of supports such as reducible oxides (TiO_2, WO_3, MoO_3, etc.) and/or through promoters (Sn, Ge, Fe, etc.) [16–19]. Other catalytic systems have been proposed (SiO_2-encapsulated SnPt) for the selective hydrogenation of crotonaldehyde to crotyl alcohol where the formation of uniform SnPt alloy phases and the pore structures in the silica layers with steric hindrance would enhance the chemo-selective hydrogenation of crotonaldehyde [20]. The most promising catalysts are those based on Ru–Sn–B [21–26]. Mizukami et al. [27] studied the performance of Ru–Sn catalysts in the selective hydrogenation of oleic acid to unsaturated alcohols and reported that the activity and selectivity of Ru–Sn catalysts prepared by sol–gel depends on the nature of the support. Costa et al. [28] found that metals promote cis–trans isomerization of the unsaturated acid, competing with the production of alcohol. Moreover, Pouilloux et al. [29] reported that the isomerization reaction of methyl oleate on Co–Sn/ZnO catalysts is produced by the Co species while the Sn species inhibits the isomerization of the olefinic bond. They also reported that the presence of ZnO does not improve this reaction. $CoSn_2$ was the active species in the reduction of methyl

* Corresponding author. Tel.: +54 342 4533858/55279; fax: +54 342 4531068.
E-mail address: pieck@fiq.unl.edu.ar (C.L. Pieck).

0926-860X/$ – see front matter © 2013 Elsevier B.V. All rights reserved.
http://dx.doi.org/10.1016/j.apcata.2013.08.014

oleate into unsaturated alcohols because the selectivity to unsaturated alcohol reached 55% at 80% of conversion [30]. As mentioned above, the direct hydrogenation of fatty acids could prevent methylation by significantly reducing raw material costs due to the non utilization of methanol. In addition, oleic alcohol is alcohol unsaturated of major commercial importance and oleic acid is a cheap, natural, renewable raw material so that today the development of selective, acid-resistant catalysts is an important issue.

In this paper, we study the influence of reaction conditions on conversion and selectivity in the selective hydrogenation of oleic acid.

2. Experimental

2.1. Catalysts preparation

γ-Al_2O_3 (Cyanamid Ketjen CK-300, pore volume = 0.5 $cm^3\ g^{-1}$, Sg (BET) = 180 $m^2\ g^{-1}$, particle size 35–80 mesh) was used as support. This material was previously calcined at 500 °C (4 h under flowing air, heating rate 10 °C min^{-1}) in order to eliminate any adsorbed contaminants.

Monometallic catalysts of Ru and Sn. Monometallic catalysts were prepared by impregnation with an aqueous solution of Ru or Sn salts. In both cases, the impregnation volume was adjusted to achieve the appropriate final concentration of each metal in the catalysts: 2.0%(w/w) Sn and 1.0%(w/w) Ru. The solutions used were $RuCl_3{\cdot}2H_2O$ (4 mg Ru cm^{-3}) and $SnCl_2{\cdot}2H_2O$ (25 mg Sn cm^{-3}). The liquids containing the Ru or Sn precursors were added to the support and the slurry was gently stirred for 1 h at room temperature and then gently heated to 80 °C to evaporate the excess liquid. The catalysts were activated by reduction in a hydrogen flow (3 h, 300 °C).

Bimetallic catalysts. The procedure used was described by Shoenmaker-Stolk et al. [31]. The support was wetted with exactly the pore volume of aqueous solution of metal precursor salts in the required amounts to achieve the desired metal content (1.0%w/w of Ru and 2.0%w/w of Sn). Wetted samples were left to stand during 12 h. A step of reduction with an excess sodium borohydryde aqueous solution was then performed. After a while, the solids were filtered and rinsed with water until acid neutrality. The last preparation step included reduction with H_2 at 300 °C, cooling, hydrogen purging and air passivation as described above.

As all the catalysts were prepared with the same support, they are labeled according to the components of the metallic function.

2.2. Determination of Ru and Sn in the catalyst

The Ru and Sn content of catalysts were determined by ICP (Perkin–Elmer, Optima 2100 DV) after acid digestion.

2.3. Temperature-programmed reduction

TPR patterns were recorded in an Ohkura TP2002 apparatus with a thermal conductivity detector. At the beginning of each TPR test, the sample was heated in air at 450 °C for 1 h. Then, it was heated from room temperature to 700 °C at a heating rate of 10 °C min^{-1} under a reducing gas stream (5% H_2 in argon).

2.4. CO chemisorption

The experiments were performed in a chemisorption equipment designed ad-hoc. The reduced catalyst was placed in a quartz reactor and first over reduced in situ in a hydrogen stream (400 °C, 1 h, 60 $cm^3\ min^{-1}$). Then the carrier was switched to N_2 and the adsorbed hydrogen was desorbed (400 °C, 60 $cm^3\ min^{-1}$) for 1 h; then, the cell was cooled down to room temperature. Then, 0.25 cm^3 pulses of diluted CO (3.5% CO in N_2) were fed to the reactor. Nonchemisorbed CO was quantitatively transformed into CH_4 over a Ni/Kieselgur catalyst and detected in a flame ionization detector connected on-line.

2.5. Fourier transform infrared absorption spectroscopy (FTIR) of chemisorbed CO

The FTIR spectra of chemisorbed CO for the prepared catalysts were recorded within a 4000–1000 cm^{-1} wavenumber range. A Shimadzu Prestige-21 spectrometer with a spectral resolution of 4 cm^{-1} was used and spectra were recorded at room temperature. Self-supported wafers with a diameter of 16 mm and a weight of 20–25 mg were used. The experimental procedure was as follows: the catalyst samples were reduced under hydrogen flow at 10 °C min^{-1} to 300 °C. Samples were then degassed at 2.7×10^{-3} Pa and 300 °C during 30 min. After recording the first (I) spectrum, the samples were exposed to a 4×10^3 Pa CO atmosphere during 5 min and then a second (II) FTIR spectrum was recorded. The chemisorbed CO absorbance for each sample was obtained by subtraction of spectra (II) and (I). Before each spectrum, a background of the gas phase was taken.

2.6. Transmission electron microscopy (TEM) measurements

TEM measurements were performed on a JEOL 2100 electron microscope operating at 200 kV with a LaB6 source and equipped with a Gatan Ultra scan camera. All the samples were embedded in a polymeric resin (spur) and cut into a section as small as 40 nm with an ultramicrotome equipped with a diamond knife. Cuts were then deposited on an Al grid previously covered with a thin layer of carbon. The microanalysis of Ru and Sn was carried out by energy dispersive X-ray spectroscopy (EDX) in the nanoprobe mode.

2.7. Cyclohexane dehydrogenation

This test reaction was performed in a fixed-bed glass reactor under the following experimental conditions: catalyst mass = 50 mg, temperature = 300 °C, pressure = 0.1 MPa, H_2 flow rate = 80 $cm^3\ min^{-1}$, cyclohexane flow rate = 1.61 $cm^3\ h^{-1}$. Before the reaction was started, the catalysts were treated in H_2 (80 $cm^3\ min^{-1}$, 500 °C, 1 h). The reaction products were analyzed in a gas chromatograph connected on-line.

2.8. Oleic acid hydrogenation tests

A stainless steel stirred autoclave (240 cm^3 effective volume) was used for these reaction tests. Operating conditions were varied one at a time, leaving the remaining ones unchanged. The standard reaction conditions chosen were: temperature, 250 °C; hydrogen pressure: 50 atm; mass of catalyst: 1 g; reactant (oleic acid) volume: 4 mL; solvent (*n*-dodecane) volume: 60 mL and stirring speed: 800 rpm. Reactant and solvent (oleic acid and *n*-dodecane) were Sigma–Aldrich 99% grade.

Reaction products were analyzed by GC (Shimadzu GC-2014) using a Chevron ZB-FFAP capillary column. The identification of reaction products was previously done by GC–MS (Shimadzu QP-5000), using the same capillary column. Only oleyl alcohol, methyl stearate, stearyl alcohol and methyl oleate were detected as significant compounds in the reactor samples. No heavy esters were found in our studies.

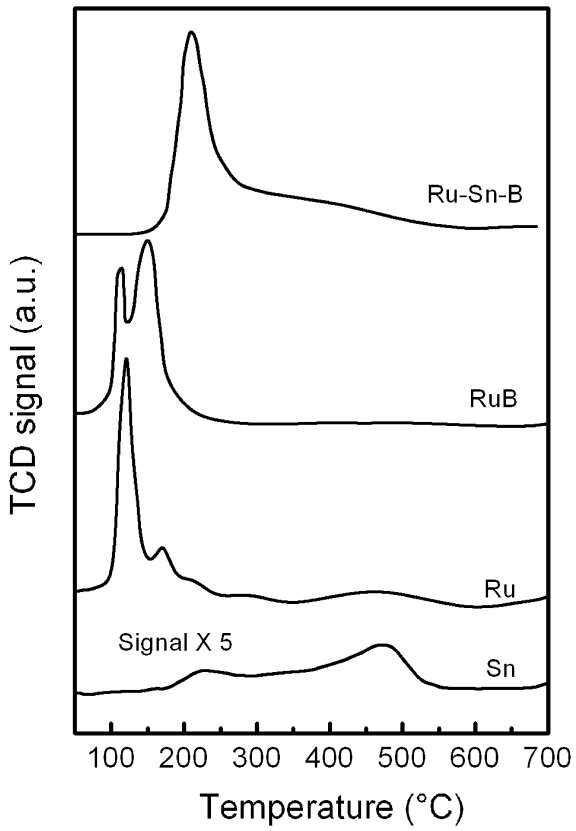

Fig. 1. TPR of the monometallic and bimetallic catalysts.

3. Results and discussion

3.1. Characterization of the catalysts

The chemical analysis of the catalysts shows metal contents in close agreement with the theoretical ones expected for all the samples.

Temperature-programmed reduction (TPR) profiles for mono and Ru–Sn–B catalysts are presented in Fig. 1. The reduction profile for the monometallic Sn catalyst is very broad (extending from 150 °C to ca 550 °C). Two reduction bands can be observed, the first at 200–300 °C and the second at 380–520 °C. The reduction pattern suggests that there exists some interaction between the Sn oxides and the alumina support. According to current understanding, Sn^{+4} species can be reduced only to Sn^{2+} due to a strong interaction with the support, which impedes further reduction to metallic Sn° [32–34].The quantitative results obtained for hydrogen consumption from the TPR spectrum of Fig. 1 indicate that ca 80% of Sn^{+4} species are reduced to Sn^{2+}. The reduction pattern corresponding to monometallic Ru catalysts also has two reduction peaks (at 120 °C and 173 °C). Similar results were reported by Echeverri et al. [23] for the reduction of $RuCl_3/Al_2O_3$. Mazzieri et al. [35] assigned the first reduction peak to the reduction of chlorinated Ru species and the smaller second peak to the reduction of oxychlorinated Ru species [36]. These arguments are based on an incomplete removal of chlorine during the calcination steps. This fraction could remain as $RuCl_3$ or other Ru–Cl species which are difficult to reduce. According to Maroto et al. [37] the use of $RuCl_3$ as a precursor leads to the presence of residual chlorine species on the surface of the catalyst, which affects H_2 and CO adsorption. The monometallic Ru–B catalyst has two reduction peaks at 110 °C and 148 °C. When compared to Ru catalysts, the main difference is that the peak attributed to Ru–Cl species is lower than the reduction to Ru oxides, while the contrary is observed for Ru catalysts without B. This could be explained considering that B favors the elimination of Cl during calcination.

Table 1
CO chemisorption, cychohexane conversion and cyclohexane conversion/CO chemisorption ratio of monometallic Ru, Ru–B and Ru–Sn–B catalysts.

Catalyst	CO/Ru	Cyclohexane conversion (%)	CH/CO
Ru	0.20	22.4	1.12
Ru–B	0.13	20.2	1.55
Ru–Sn–B	0.07	1.7	0.24

CH/CO: cyclohexane conversion/CO chemisorption.

The bimetallic catalyst modified by the addition of B has a unique peak with a maximum at 208 °C and a long tail extending up to 500 °C. The well-defined zone of the peak can be attributed to the co-reduction of Ru and Sn [38] and the long tailing band (200–500 °C) to Sn species segregated from Ru. The behavior of the Ru–Sn system is in this sense similar to that found in supported Pt–Re catalysts which has been explained as a promotional effect by Pt on the reduction of Re [39,40].

The dispersion of the catalysts was obtained by chemisorption of CO a room temperature. Preliminary results show that CO is chemisorbed only on Ru, while Sn and B do not chemisorb CO. The dehydrogenation of cyclohexane is a typical metal catalyzed, non-demanding reaction (it does not require the presence of particular atom ensembles) [41] being only Ru active. Table 1 shows that B addition sligtly decreases CO chemisorption and cyclohexane dehydrogenation while Sn produces a big decrease of dehydrogenation and chemisorption. The changes of the CH/CO ratio could be attributed to a modification of the electronic structures of the Ru catalyst by B and Sn. It is known that Sn influences the activity on cychlohexane dehydrogenation of the metal function due to a geometric effect and/or a change in the electronic structure of the active metal [33].

The metallic particle size was additonaly studied by TEM. It was found that monometallic Ru catalyst have a homogeneous distribution of particles with sizes between 0.7 and 1.3 nm. The bimetallic Ru–Sn–B catalyst has particles between 1 nm and 3 nm with two types of aggregates, rich in Ru and rich in Sn. Fig. 2 shows representative TEM images of Ru and Ru–Sn–B catalysts.

The metal interaction was also studied using the FTIR-adsorbed CO technique. As pointed out above, CO adsorbs on Ru metallic sites but not on Sn sites. The FTIR spectra of chemisorbed CO are shown in Fig. 3 for the Ru catalysts. The recorded spectra are presented only in the 1800–2200 cm^{-1} wavenumber range which is the relevant one, and the main band at 2038–2042 cm^{-1} that appears in all catalysts spectra is attributed to the linear adsorption of CO on Ru° [42–44]; the lower wavelength bands could be due to the presence of polycarbonyl species $Ru^{\delta+}(CO)_x$.[45–47]. For the monometallic Ru catalysts, the characteristic Ru°–CO band at 2042 cm^{-1} is accompanied by lower wavelength bands located around 2133 and a shoulder at 2080 cm^{-1}. These bands may be due to the presence of $Ru^{\delta+}$ in chlorinated species [48]. Such a type of bands has been found in Ru carbonyl halides with several oxidation states [49]. It has been reported [50] that $Ru_2(CO)_6Cl$ has two bands at 2143 cm^{-1} and 2083 cm^{-1}. The spectra of Ru–B catalysts shows essentially the same peak as Ru catalysts, but the peak attributed to Ru°–CO is shifted to 2052 cm^{-1}; moreover, the peak due to Ru chloride species is also shifted to 2133 cm^{-1}. This means that B is in strong interaction with Ru°. It is expected that the peak due to Ru°–CO shifts to a lower frequency because B has a lower electronegativity than Ru. The shift observed could be attributed to B which is not reduced to metallic state and produces a charge transfer from Ru atoms. The spectra recorded for the Ru–Sn–B catalyst is not only reduced in intensity (possibly due to a blocking effect on Ru sites by Sn) but is

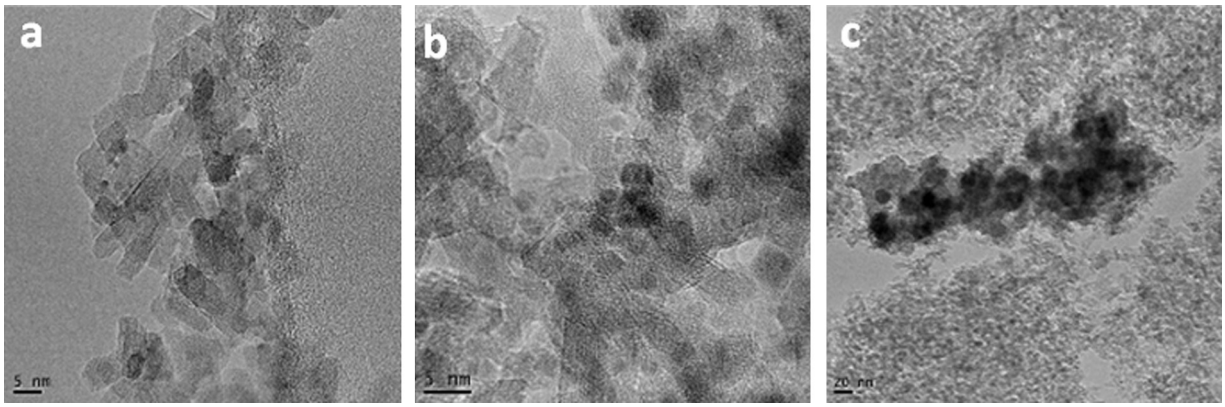

Fig. 2. Representative TEM images of Ru/Al_2O_3 catalysts (a), $Ru–Sn–B/Al_2O_3$ catalysts region rich in Ru (b), and $Ru–Sn–B/Al_2O_3$ catalysts region rich in Sn (c).

profoundly modified: the 2143 cm^{-1} band completely disappears and the 2076 cm^{-1} band becomes more important. These modifications could reflect a strong modification in the electronic structure and the presence of small quantities of Ru^{n+} species.

Additional characterizations of $Ru–Sn–B/Al_2O_3$ catalysts by XPS techniques were previously reported [51]. It was reported that the Ru–Sn–B catalyst has a higher proportion of Ru and Sn on its surface than the corresponding bulk concentration. Moreover, Ru and Sn are only partially reduced to the metallic state. The major part of Sn^{4+} reduced to Sn^{2+} is strongly stabilized by interaction with the alumina support. A single peak of B 1s found at 192.8 eV can be attributed to B^{3+}, possibly in the form of sodium borate adsorbed on the alumina support near the Ru clusters. In the B 1s spectrum, no peak around 187 eV was observed, indicating the absence of metal boride in the present catalyst system. This is confirmation that after FTIR-CO treatment (H_2, 300 °C) B is not reduced to the metallic state. The −0.5 eV shift observed in the bond energy of B^{3+} implies an increase in its electronic density, possibly due to a charge transfer from Ru atoms.

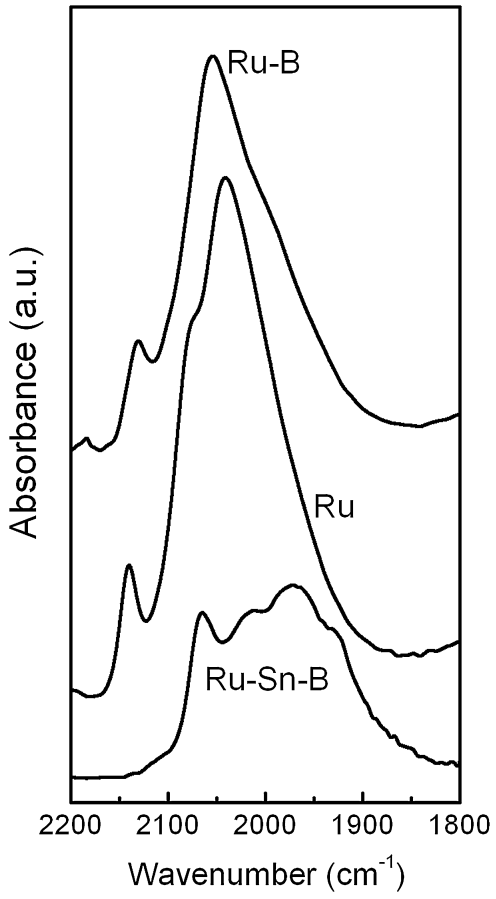

Fig. 3. FTIR spectra of CO adsorbed on Ru, Ru–B and Ru–Sn–B catalysts at 30 Torr.

3.2. Activity and selectivity of the Ru–B and Ru–Sn–B catalysts on the hydrogenation of oleic acid

The Ru–B catalyst has high activity for hydrogenated oleic acid but unfortunately the selectivity to oleyl alcohol is zero even at low reaction time. On the other hand, the Ru–Sn–B catalyst has higher selectivity but lower activity. The higher selectivity to oleyl alcohol of the Ru–Sn–B catalyst compared to Ru–B and Ru catalysts could be attributed to a strong interaction between Ru and Sn species as it was found to affect the Ru electronic and catalytic properties. Klusoň and Červený [17] proposed that the highest activity and selectivity are attributed to Ru° sites interacting with Sn^{2+} or Sn^{4+} Lewis acid sites via oxygen, wherein the Lewis acid preferentially activates C=O, facilitating the hydrogen transfer from adjacent Ru–H sites.

For the sake of simplicity, the hydrogenation results of the Ru–B catalyst are not shown and discussed because there is no formation of the desired product (oleyl alcohol).

3.3. Influence of operating conditions on the selective hydrogenation of oleic acid on the Ru–Sn–B catalyst

Some exploratory reaction runs were first made to reveal the possible existence of external and internal diffusional limitations. Those experiments were done at 270 °C and 50 atm, and the reactor was initially charged with 1 g of catalyst, 4 mL of oleic acid and 60 mL of dodecane (solvent). Three agitation levels were used: 546, 800 and 1096 rpm. The results show that in this range the agitation speed does not have any significant influence on conversion values. Neither were the product distribution patterns significantly modified as the agitation level varied (results not shown). The virtual independence of results on stirring speed indicates negligible external mass transfer effects on reaction rates. Therefore, a stirring speed of 800 rpm was chosen as standard for all kinetic experiments.

Internal diffusive effects can be assessed using the classical Weisz–Prater criterion [52]:

$$\phi = \frac{robs\rho p.d_p^2}{36.C_S D_{eff}} \leq 0.3$$

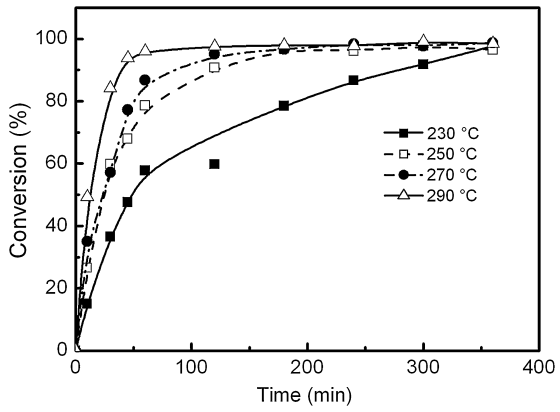

Fig. 4. Oleic acid conversion as a function of time at several reaction temperature levels.

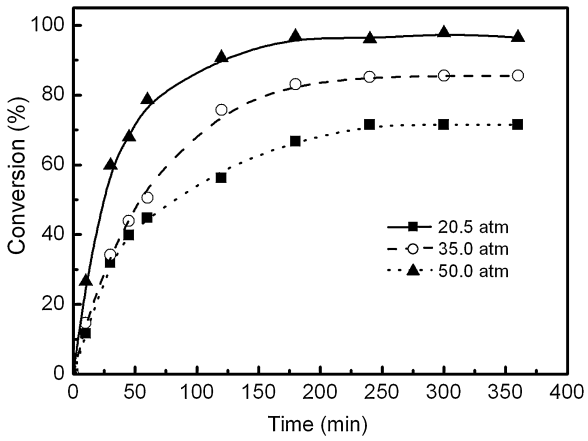

Fig. 6. Oleic acid conversion as a function of time at different operating pressures.

Rates of oleic acid consumption were calculated from the slope of conversion versus time plots (Fig. 4). The highest value was found at 290 °C, extrapolated to zero conversion, it was 1.53 10^{-5} gmol s^{-1} g^{-1}. From the support porosity and a value of 3.65 g cm^{-3} for the density of solid γ-Al_2O_3, the catalyst particle density (ρ_p) was computed as 1.29 g cm^{-3}. The mean catalysts particle size (d_p) corresponding to the used sieving range was 0.034 cm. The highest rate observed was an initial (i.e. zero time) rate so that the oleic acid concentration at the catalyst surface (C_s), calculated from the oleic acid/solvent ratio in the mixture charged to the reactor, was 1.969×10^{-4} mol cm^{-3}. The molecular diffusivity of oleic acid was assumed equal to methyl oleate due to the similar molecule size and morphology. Considering the values of particle density and porosity and that the molecular diffusivity of methyl oleate is 1.89×10^{-5} cm^2 s^{-1} [31], the effective diffusivity was 1.29×10^{-5} cm^2 s^{-1}. A value of $\phi = 0.24$ was finally obtained, and the absence of significant internal diffusive effects was ascertained [52].

3.3.1. Influence of reaction temperature

Several kinetic runs were done within the 230–290 °C temperature range. Conversion values increase, as expected, when the temperature level rises (Fig. 4). The results of yield to oleyl alcohol are shown in Fig. 5. The formation of oleyl alcohol goes through a maximum at some intermediate run time. At higher reaction times, the oleyl alcohol formed by the selective hydrogenation of oleic acid is fully hydrogenated to the corresponding saturated fatty alcohol (stearyl alcohol). Higher yields are achieved at 290 °C. At higher temperatures (290 °C), the hydrogenation rate noticeably increases so the intermediate oleyl alcohol is rapidly transformed into stearyl alcohol, which is a final product. These results could be explained taking into account that activation energies associated with hydrogenolytic-type reactions are usually higher than for simple C=C bond hydrogenations. When the reaction temperature increases, the rate of transformation of oleic acid to fatty alcohols is favored over the simple double bond hydrogenation. However, at higher temperature, the C=C double bond is also hydrogenated producing stearic acid. On the other hand, stearic acid is an intermediate whose amount never reaches high values.

3.3.2. Influence of hydrogen pressure

The effect of hydrogen pressure was explored at 20.5, 35 and 50 atm. The temperature was kept at 250 °C and charge characteristics and stirring speed were set at the same values as in the preceding paragraph. Fig. 6 shows that oleic acid conversion strongly increases when hydrogen pressure rises from 20.5 upto 50 atm. Moreover, the hydrogen pressure has a marked effect on the yield to oleyl alcohol (Fig. 7). The yield to oleyl alcohol continuously increases with the reaction time when the reaction is performed at low pressure (20.5 and 35 atm) but at higher pressure (50 atm), the oleyl alcohol yield goes through a maximum in the first hour of reaction. These results reflect a compromise between the formation of the unsaturated alcohol and the hydrogenation of its C=C double bond at higher pressures.

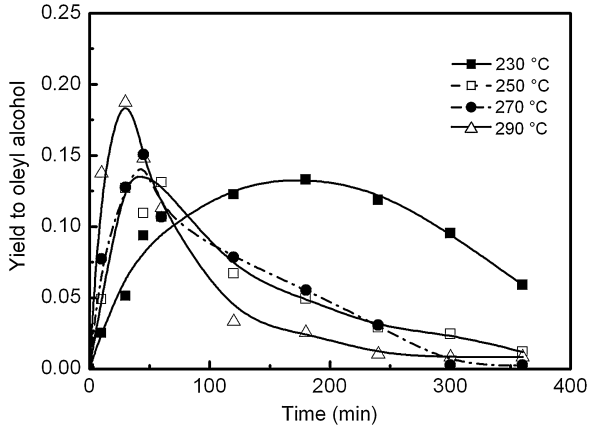

Fig. 5. Yield to oleyl alcohol as a function of time at several reaction temperature levels.

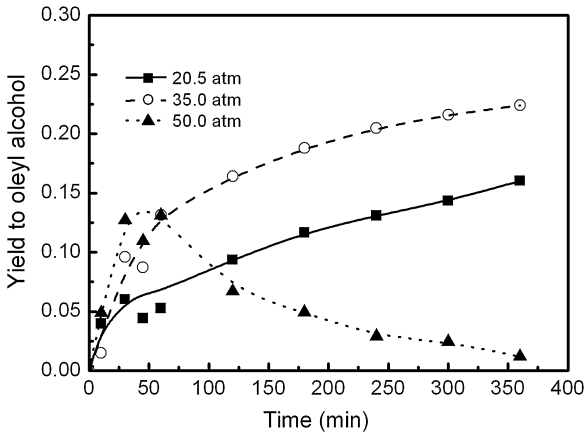

Fig. 7. Yield to oleyl alcohol as a function of time at different operating pressures.

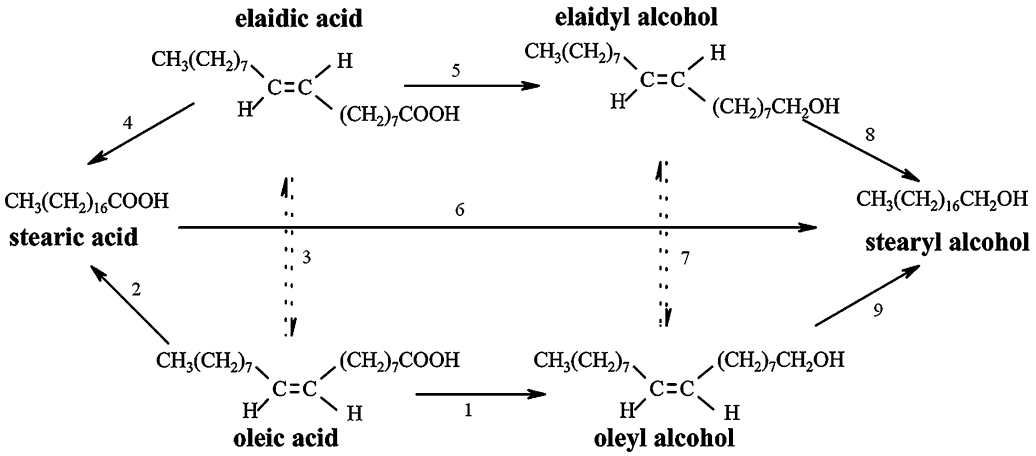

Scheme 1. Reaction scheme for the hydrogenation of oleic acid [48].

3.3.3. Simplified kinetic model

In order to give a more rational basis to the analysis of the kinetic data obtained, a simple reaction model was formulated, which was based on the reaction scheme proposed by Mendes et al. [53] for the selective hydrogenation of oleic acid which is presented in Scheme 1. As shown, the possible primary reactions are: (1) the hydrogenation of the carboxylic group into unsaturated oleyl alcohol; (2) the hydrogenation of the C=C bond into saturated stearic acid; (3) the isomerization of the C=C bond into the trans elaidic acid. Despite the numerous kinetic models developed for fats and oils hydrogenation and the existence of reasonable reaction pathways for the selective hydrogenation of carbonyl groups, no such studies are found in the literature.

No heavy esters were found in our studies. Our kinetic model proposal is a very simple one with only four components (oleic acid, oleyl alcohol, stearic acid and stearyl alcohol). The cis–trans isomerization reactions are not considered, elaidic acid and oleic acid are taken as oleic acid and elaidyl alcohol and stearyl alcohol are named as stearyl alcohol. The kinetics for each model step are supposed to be first order and irreversible, and the effect of hydrogen is not taken into account explicitly and is assumed to be somehow included in rate constants. Another reasonable simplification would come from the chemical similarity of oleic acid/stearic acid and oleyl alcohol/stearyl alcohol molecules. Regarding the selective hydrogenation of oleic acid to its corresponding alcohols, the presence or absence of a double bond far from the terminal carboxylic group to be hydrogenated should not influence this reaction rate significantly. The rate constants for the C=C double bond hydrogenation should not depend much on the presence of a remote COO— or OH— group. Therefore, the proposed model has only two rate constants: one for the selective hydrogenation of carbonyl groups ($k_{C=O}$) and the other for the C=C double bond hydrogenation ($k_{C=C}$).

$$\frac{dn_A}{dt} = -(k_{C=O} + k_{C=C})n_A$$

$$\frac{dn_B}{dt} = -(k_{C=O}n_B + k_{C=C})n_A$$

$$\frac{dn_C}{dt} = -(k_{C=O}n_C + k_{C=C})n_A$$

where $k_{C=O}$ = kinetic constant for the —COOH group hydrogenation $k_{C=C}$ = kinetic constant for the C=C group hydrogenation n_A, n_B and n_C are the oleic acid, stearyl acid and oleyl alcohol mole numbers, respectively.

This differential equations system is readily solved to get:

$$\ln(Y_C + Y_A) = -k_{C=C}t$$

$$\ln(Y_A) = -(k_{C=O} + k_{C=C})t$$

where Y_A = molar fraction of oleic acid within the reaction products. Y_C = molar fraction of oleyl alcohol within the reaction products. t = reaction time (s)

The experimental points to correlate the kinetic model were taken for a reaction time lower than 180 min in order to eliminate any possible deactivation interference. Values of kinetic constants obtained from regression analysis of experimental data are presented in Fig. 8. The corresponding activation energies for both reaction types can also be determined, its values being $E_{C=O}$ = 67 kJ mol^{-1} and $E_{C=C}$ = 43 kJ mol^{-1}. In a previous work, we reported 116 and 56 kJ mol^{-1} for the hydrogenation to methyl oleate [54]. It seems that the reduction of a carboxylic group is easier than the ester group. Moreover, these values are close to 103 kJ mol^{-1} reported by Coenen et al. [55] for the formation of unsaturated fatty alcohols.

Table 2 shows the values of the kinetic constants of reaction at the three pressure levels explored. It shows that the kinetic constant increases with pressure of H_2 indicating that the reaction depends on the amount of H_2 dissolved in the reactant medium. These kinetic "constants" should include some hydrogen pressure term which arises from the absence of a hydrogen concentration

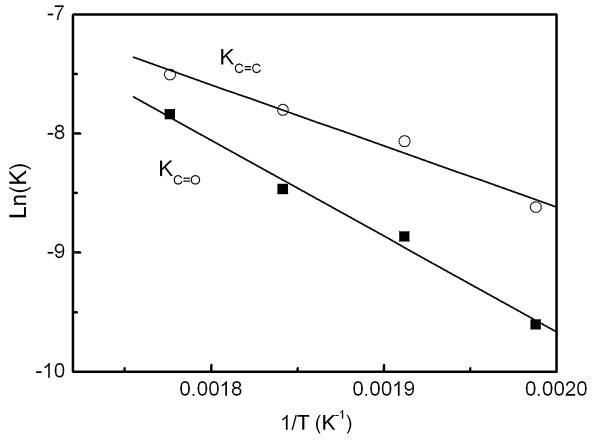

Fig. 8. Arrhenius plots of estimated rate constants.

Table 2
Values of kinetic constant as a function of the operating pressure.

Pressure (atm)	$K_{C=C}$ (s^{-1})	$K_{C=O}$ (s^{-1})
20.5	1.5×10^{-4}	2.4×10^{-5}
35.0	1.5×10^{-4}	7.0×10^{-5}
50.0	3.1×10^{-4}	1.4×10^{-4}

term in the kinetic expressions used in the simple model. A positive effect of pressure on the constant values is expected.

4. Conclusions

The characterization results clearly show a strong interaction between Ru and Sn. The electronic and catalytic properties of Ru are modified by their interaction with Sn and B. The incorporation of Sn leads to catalysts capable of producing oleyl alcohol from oleic acid. The Ru or Ru–B catalysts are not selective to produce oleyl alcohol.

The experiments of oleic acid hydrogenation showed that an increase in reaction temperature leads to an increase in activity while the yield to oleyl alcohol goes through a maximum. This is because the reaction of hydrogenation of the C=C double bond have a lower activation energy than C=O reduction reactions. The increase in operating pressure has a positive effect on conversion and a more important effect on selectivity. A very simple first order kinetic model, which can be useful to compare catalyst performance more rationally, is proposed and reasonably represents the results obtained.

Acknowledgments

Thanks are given to Elsa Grimaldi for the English language editing.

References

[1] H.J. Richter, J. Knaut, J. Am. Oil Chem. Soc. 61 (1984) 160–175.
[2] W. Rittmeister, US Patent 3,193,586 (1965).
[3] H. Rutzen, W. Rittmeister, US Patent 3,729,520 (1973).
[4] G. Demmering, H. Schütt, H. Rutzen, DE-AS Patent 2,513,377 (1975).
[5] J. Cieslar, W. Bulanda, Przem. Chem. 63 (1984) 375–381.
[6] H. Bertsch, H. Reinheckel, K. Haage, Fette, Seifen, Anstrichm. 66 (1964) 763–773.
[7] H. Bertsch, H. Reinheckel, K. Haage, Fette, Seife, Anstrichm. 71 (1969) 357–362.
[8] H. Bertsch, K. Haage, H. Reinheckel, Fette, Seifen, Anstrichm. 71 (1969) 851–857.
[9] K. Lindner, Tenside Textilhilfsmittel Waschrohstoffe, vol. I, 2nd edn, Wissenschaftl. Verlags GmbH, Stuttgart, 1964, pp. 144.
[10] J.W.E. Coenen, Fette, Seifen, Anstrichm. 77 (1975) 431–464.
[11] G. Qualeatti, D. Germanas, US Patent 4,340,546 (1982).
[12] G. Qualeatti, D. Germanas, US Patent 4,446,073 (1984).
[13] K. Kokubo, K. Tsukada, Y. Miyabata, Y. Kazama, JP Patent 58,210,035 (1983).
[14] K. Tsukada, Y. Miyabata, JP Patent 5,995,227 (1984).
[15] K. Tsukada, Y. Miyabata, K. Fukuoka, JP Patent 59,106,431 (1984).
[16] P. Klusoň, L. Červený, Appl. Catal. A 128 (1995) 13–31.
[17] P. Klusoň, L. Červený, Chem. Listy 91 (1997) 100–104.
[18] S.A. da, S. Corradini, G.G. Lenzi, M.K. Lenzi, C.M.F. Soares, O.A.A. Santos, J. Non-Crystalline Solids 354 (2008) 4865–4870.
[19] G. Luo, S. Yan, M. Qiao, J. Zhuang, K. Fan, Appl. Catal. A 275 (2004) 95–102.
[20] K. Taniya, C.H. Yu, S.C. Tsang, Y. Ichihashi, S. Nishiyama, Catal. Commun. 14 (2011) 6–9.
[21] P. Gallezot, D. Richard, Catal. Rev. Sci. Eng. 40 (1998) 81–126.
[22] T. Miyake, T. Makino, S. Taniguchi, H. Watanuki, T. Niki, S. Shimizu, Y. Kojima, M. Sano, Appl. Catal. A 364 (2009) 108–112.
[23] D.A. Echeverri, J.M. Marín, G.M. Restrepo, L.A. Rios, Appl. Catal. A 366 (2009) 342–347.
[24] S. Taniguchi, T. Makino, H. Watanuki, Y. Kojima, M. Sano, T. Miyake, Appl. Catal A 397 (2011) 171–173.
[25] A. Piccirilli, Y. Pouilloux, S. Pronier, J. Barrault, Bull. Soc. Chim. Fr. 132 (1995) 1109–1114.
[26] V.M. Deshpande, K. Ramnarayan, C.S. Narasimhan, J. Catal. 121 (1990) 174–182.
[27] K.Y. Cheah, T.S. Tang, F. Mizukami, S. Niwa, M. Toba, Y.M. Choo, J. Am. Oil Chem. Soc. 69 (1992) 410–416.
[28] C.M.M. Costa, E. Jordão, M.J. Mendes, O.A.A. Santos, F. Bozon-Verduraz, React. Kinet. Catal. Lett. 66 (1999) 155–162.
[29] K. Oliveira Vigier, Y. Pouilloux, J. Barrault, J. Mol. Catal. 306 (2009) 102–106.
[30] K. Oliveira Vigier, Y. Pouilloux, J. Barrault, Catal. Today 195 (2012) 71–75.
[31] M. Shoenmaker-Stolk, J. Verwijs, J. Scholten, Appl. Catal. 30 (1987) 339–352.
[32] R. Burch, J. Catal. 71 (1981) 348–359.
[33] V.A. Mazzieri, J.M. Grau, J.C. Yori, C.R. Vera, C.L. Pieck, Appl. Catal. A 354 (2009) 161–168.
[34] B.A. Sexton, A.E. Hughes, K. Foger, J. Catal. 88 (1984) 466–477.
[35] V.A. Mazzieri, F. Coloma-Pascual, A. Arcoya, P.C. L'Argentière, N.S. Fígoli, Appl. Surf. Sci. 210 (2003) 222–230.
[36] A. Bossi, F. Garbassi, A. Orlandi, G. Petrini, L. Zanderighi, Stud. Surf. Sci. Catal. 3 (1979) 405–416.
[37] A. Maroto, M. Cerro, A. Guerrero, I. Rodríguez, Appl. Catal. A 283 (2005) 23–32.
[38] Y. Pouilloux, F. Autin, C. Guimon, J. Barrault, J. Catal. 176 (1998) 215–224.
[39] B.H. Isaac, E.E. Petersen, J. Catal. 85 (1984) 8–15.
[40] L. Chen, Y. Li, J. Zang, H. Luo, S. Cheng, J. Catal. 145 (1994) 132–140.
[41] M. Boudart, A. Aldag, J.E. Benson, V.A. Dougharty, C.G. Harkings, J. Catal. 6 (1966) 92–99.
[42] K. Kostov, H. Rauscher, D. Menzel, Surf. Sci. 278 (1992) 62–86.
[43] F.M. Hoffmann, M.D. Weisel, Surf. Sci. 269–270 (1992) 495–499.
[44] W.K. Kuhn, J.W. He, D.W. Goodman, J. Vac. Sci. Technol. A 101 (1992) 2477–2486.
[45] K. Hadjiivanov, J.C. Lavalley, J. Lamotte, F. Maugé, J. Saint-Jus, M. Chez, J. Catal. 176 (1998) 415–425.
[46] G.H. Yokomizo, C. Louis, A.T. Bell, J. Catal. 120 (1989) 1–14.
[47] J.A. de los Reyes, M. Vrinat, M. Breysse, F. Mauge, J.C. Lavalley, Catal. Lett. 13 (1992) 213–219.
[48] T. Narita, H. Miura, K. Sugiyama, T. Matsuda, R.D. Gonzalez, J. Catal. 103 (1987) 492–495.
[49] J.L. Robbins, J. Catal. 115 (1989) 120–131.
[50] E.A. Seddon, K.R. Seddon, The chemistry of ruthenium, in: R.J.H. Clark (Ed.), Topics in inorganic and general chemistry, Elsevier Science Publishers B.V., Netherlands, 1984 (chapter 3).
[51] M.A. Sánchez, V.A. Mazzieri, M.R. Sad, R. Grau, C.L. Pieck, J. Chem. Technol. Biotechnol. 86 (2011) 447–453.
[52] M.A. Vannice, Kinetic of Catalytic Reactions, Springer, New York, 2005, pp. 61–86.
[53] M.J. Mendes, O.A.A. Santos, E. Jordão, A.M. Silva, Appl. Catal. A 217 (2001) 253–262.
[54] M.A. Sánchez, V.A. Mazzieri, M.R. Sad, C.L. Pieck, React. Kinet. Mech. Catal. 107 (2012) 127–139.
[55] J.O. Coenen, Seifen-Öele-Fette-Wachse 14 (1975) 341.